Climate of the weakly-forced yet high-impact convective storms throughout the Ohio River Valley and Mid-Atlantic United States

Binod Pokharel[1,2], S.-Y. Simon Wang[1,2], Jonathan Meyer[1,2], Robert Gillies[1,2], and Yen-Heng Lin[2]

[1]Utah Climate Center, Utah State University, Logan, Utah, USA

[2]Department of Plants, Soils, and Climate, Utah State University, Logan, Utah, USA

Abstract

The 1-in-1000-year precipitation event in late June 2016 over West Virginia caused tremendous flooding damage. Like the 2012 mid-Atlantic derecho that blacked out much of the D.C. area, similar events can be traced to small, mid-tropospheric perturbations (MPs) embedded in the large-scale ridge pattern. Under this "weakly-forced" pattern, severe weather outbreaks commonly occur alongside eastward propagating MPs acting as a triggering mechanism for progressive mesoscale convective systems, which move across the central and eastern U.S. Forecasting of such weakly-forced yet severe weather events is difficult in both weather and climate timescales. The present diagnostic analysis of the MP climatology is the first step toward developing metrics that can identify and evaluate weakly-forced severe weather outbreaks in multi-model projections. We report a discernable, potentially pronounced subseasonal change in the MP climatology associated with the changing climate of North America. Both sea surface temperatures within the Gulf of Mexico and mid-level high pressure over the central U.S. were found to exhibit strong correlations with MPs. Analysis of regional climate downscaling indicates a projected increase in MP frequency and the associated convective precipitation through the mid 21st century.

1. Introduction

In mid-summer over the central United States (U.S.), convective storms tend to be sustained for a long time as they propagate across the Ohio River Valley and even through the mid-Atlantic states. While it is generally recognized that organized convective storms are associated with strong synoptic low pressure systems featuring large-scale baroclinic forcing, a unique type of mid-summer storm occurs under northwesterly flow associated with high pressure ridges (Johns 1982, 1984, 1993). Both types of storm environments can produce severe weather, but the northwesterly flow (NWF) storms, which are also called ridge rollers (Galarneau and Bosart 2005), are known to induce outbreaks of propagating convective windstorms or derechos (Johns and Hirt 1987; Bentley and Mote 1998). This NWF synoptic setting presents a particular challenge for numerical weather prediction models primarily due to the fact that the storm environment is so weakly forced in terms of baroclinicity compared to the low pressure case.

Mid-level flow-terrain interactions over the Rocky Mountains plays an important role in creating atmospheric disturbances that propagate over long distances within the steering synoptic northwesterly flow (Wang et al. 2011b). The majority of the synoptic northwesterly flow severe weather outbreaks can be linked to pre-existing perturbations that originated from the northeastern Rocky Mountains, referred to as mid-tropospheric perturbations (MPs, Wang et al. 2009, 2011a, 2011b). MPs provide middle- to lower-tropospheric instability and steering for travelling convective storms and are responsible for 60% of convective storms with wind and hail (Wang et al., 2011a). Thus, any climate variations that may affect MP genesis and steering would be expected to be linked to variations in synoptic northwesterly flow severe weather outbreaks. Another important part of this study examined the future projection of the North American synoptic setting where these ridge type systems could bring extreme weather events.

By tracking and examining the long-term variations in MP's using regional and global reanalysis datasets, the analysis presented here offers diagnostic insight into these convective triggers. In addition to the observation-based reanalysis data, this study explores future downscaled regional climate projections of MPs and associated severe weather events. However, the examination of mesoscale features and frequencies of convective storms in the historical reanalysis and future climate projections is difficult due to biases in model precipitation and thermodynamic variables. Therefore, a set of kinematic metrics was developed to aid in the diagnosis. In our quest to address the question as to why some northwesterly flow events produce MPs that propagate downstream and initiate severe weather while others do not, an examination of MP frequency and the corresponding background flow was undertaken – more specifically to what extent an ambiguous ridge or synoptic northwesterly flow pattern, given its weak convective forcing, can sustain MP propagations and so, promote storm development. The following sections sequentially put forward a description of two recent MP-led convective storms that were extreme and high-impact (Section 2), the data and methodologies used (Section 3), followed by the MP climatology and variability (Section 4) and ended with discussion and a summary in Section5.

2. Recent Extreme Events

In June 2016, in the presence of a continental-scale upper-level ridge, the NWF synoptic environment produced two extreme weather events on opposite ends of the continental U.S., bringing record flooding in West Virginia and scorching heat conditions in the Southwest (Di Liberto 2016). In order to highlight the connection between the strong anticyclone and the northwesterly flow, Figure 1a shows an overlay of 600-hPa wind vectors and storm report frequency (cataloged by the Storm Prediction Center (SPC)) for 21-24 June 2016. Of note is that along the northern edge of the ridge centered over the central plains, a series of shortwaves formed in the mid-troposphere and subsequently propagated across the Ohio valley and then into West Virginia. This singularity produced a "1-in-1000-year" precipitation event with subsequent record-breaking floods (Grote and Dyer 2017; Corrigan et al. 2017; Perfater et al. 2017). The D.C./Mid-Atlantic derecho event of 2012 was another severe weather outbreak associated with NWF synoptic conditions (Figure 1b) (Šepić and Rabinovich 2014). The prevailing ridges that were present in both June 2012 and 2016 events brought exceptionally dry weather conditions that lead to moderate-to-exceptional droughts across the continental U.S. In the Southwest, both events were ranked as the warmest June in history with several high temperature records (NOAA 2016; Mo and Lettenmaier 2015).

In the case of June 2016, the continental-scale ridge was well predicted by weather models but with the exception of a few high-resolution ensemble models (Schwartz et al. 2015), the storms and associated extreme precipitation were not well forecast (Corrigan et al. 2017; Grumm 2017); thus highlighting a shortfall in meteorological forecast models to capture weakly-forced convective storms. Moreover, climate projection studies fail to capture northwesterly synoptic flow severe weather outbreaks (e.g., Weaver et al. 2016; Feng et al. 2016; Feng et al. 2012; Jiang et al. 2006; Berg et al. 2015).

3. Data Sources and Methodology

3.1 Reanalysis data

Because of its high spatial resolution compared to global reanalysis we used 3-hourly North American Regional Reanalysis (NARR, Mesinger et al. 2006) data to calculate the MPs. NARR compares well with observations (Mesinger et al. 2006) and has been shown to resolve the type of sub-synoptic scale features associated with MPs (Wang et al. 2011b). We also utilized NCEP/NCAR reanalysis R1 data (Kalnay et al. 1996) to resolve hemispheric-scale atmospheric circulations but due to the coarser resolution, NCEP data was not considered for the MP calculation. Following Johns (1982), severe weather ground truth for this study was supplied by storm reports compiled from the Warning Coordination Meteorologist (WCM) page hosted by the SPC (http://www.spc.noaa.gov/wcm/). However, storm observations originate from personnel sightings which, due to various motivations etc., presents data quality issues (Weiss et al. 2002; Gallus et al. 2008). Hence, a diagnostic metric based on MPs was an essential component of our analysis. Furthermore, the use of NARR data was elemental in the construction of the climatology of MPs. This was implemented for the months of June and July when ~80% of northwestern flow events occur as well as those that propagate furthest (Johns 1984, 1993).

3.2 Regional Downscaled Modeling Data

In order to examine future climate projections, the North American Regional Climate Change Assessment Program (NARCCAP) regional climate model simulations (Mearns et al. 2007) were used to calculate the MP. The NARCCAP data consist of historical (1968-1999) and future (2038-2069) periods and has seven different simulations with two different global model forcing for each regional model (defined as "global model-driven"). The future run was forced with the A2 emission scenario of Special Report on Emission Scenarios (SRES, Nakicenovic et al. 2000) for the mid 21st century. However, only six simulations (three models) listed in Table 1 offer the required 3-hourly variables necessary to calculate MPs. The ensembles of these six simulations were used for the diagnosis of MPs and associated convective precipitation. For verification purpose, we used three historical simulations (CRCM, MM5I and WRFG) that were forced by the NCEP reanalysis data over the period of 1980-2003 to calculate the MPs (defined as "reanalysis-driven"). Given the broad agreement between the climatology depicted by these NCEP-driven simulations and that of NARR as well as their similar spatial resolutions (Wang et al. 2009), the comparison of these with the NARR analysis provides a validation perspective on the climatology and variations in MPs.

3.3 Mid-tropospheric perturbation (MP) tracking

To depict northwesterly flow (NWF) events, three criteria were defined in order to filter out the region of interest. The first (called 'circulation criteria') excludes regions of large-scale troughs of low-pressure and was accomplished by calculating the stream function while removing the global mean. The circulation criterion excludes regions that feature negative stream function values, which denotes troughs. Since mid- and upper-level winds play an important role in the propagation of MPs further downstream, a second criteria (called 'wind criteria') was aimed to exclude regions of weak winds, hence only those regions of wind speed greater than 15 ms^{-1} averaged at mid- and upper-levels (600-hPa and 250-hPa) were selected. Lastly, a third criteria (called 'moisture criteria') identifies regions of high humidity as dry vortices alone cannot generate widespread severe weather (Wang et al. 2011a). As noted earlier, the use of vertically integrated precipitable water was adopted from various perspectives:

i. Precipitable water is commonly used for the probable maximum precipitation forecasting (Tetzlaff and Zimmer 2013).

ii. Precipitable water is a good means of estimating regions of moist vortices and resulting convection.

MPs were identified from mid-level wind and relative vorticity fields at 600-hPa. To ensure definitive identification, the MPs were isolated using three methods (approaches): First calculated, was the root-mean-square of the relative vorticity. Next, given that the average life cycle of MPs is 48-hours (Wang et al. 2011a), the vorticity fields were subjected to both low- and high-pass temporal filters considering nine-point weighted and seven-point running average, respectively, to isolate the MPs general lifecycle. Since moisture is an important aspect in convective environments, the other two approaches considered moisture. First was the consideration of upper tropospheric moisture. After applying the same high- and low-pass temporal filters to 300-hPa specific humidity, the covariance of the filtered vorticity and 300-hPa specific humidity was evaluated. Lastly, the vertically integrated precipitable water, likewise temporally filtered, was determined and the covariance between the filtered vorticity and precipitable water fields computed. For all fields, the study undertook the examination of weekly averages for the months of June and July, i.e. the MP high season (Wang et al. 2011a). Several thresholds of precipitable water were tested before concluding that 24mm was a threshold capable of identifying MPs. Finally, it should be noted that all three exclusion criteria were applied before computing the root-mean-square of vorticity and the covariances of vorticity and humidity. Given the third approach already accounts for precipitable water (PW), only the circulation criteria and wind criteria were applied to the covariance of vorticity and PW. The result of our multi-variable approach to MP identification is shown over a 32-year climatology (1985-2016) in Figure 2. All three approaches show similar patterns where MPs originate east of the Rockies and propagate to the east. However, the third approach in July (Figure 2f) shows that

MPs originate further inside of the Rockies, a deviation from the MP tracks defined by Wang et al. (2011a, b).

For the comparison between MPs and storm frequency, SPC storm reports, which considered wind, hail and tornado reports, were first projected onto a 1^{o} X 1^{o} grid. Initial examination of our MP identification using the gridded storm reports shows the first approach using the root-mean-square (RMS) of relative vorticity performed the best (i.e. capturing the majority of the storm occurrence). In addition, the RMS of vorticity shows the representation of severe weather condition for three cases discussed in Section 4.1. Based on the comparison for case analysis and climatology, from the three approaches, the first approach using circulation criteria, hereafter referred to as the "MP frequency" performed the best and is considered for the remainder of the analysis presented in this study. Furthermore, the NWF region where the MP frequency propagate is hereafter referred to as the 'MP corridor'.

4. MP Characteristics and Climatology

4.1 Case Verification

The application of MP metrics on the depiction of NWF severe weather outbreaks is first tested by examining the recent extreme cases of the 2016 West Virginia flood and the 2012 Mid-Atlantic derecho, both occurring in late June. During the course of four days, both events produced similar patterns of storm reports consisting of hail, gusty winds and tornadoes (Figure 1). To focus our analysis on these two events, the MP identification process is averaged over 27-30 June 2012 and 21-24 June 2016 to capture the evolution of the atmosphere leading up to the outbreak. The result shows a good agreement between the storm frequency (Figure 1) and MP frequency (Figure 3) along the NWF.

One noticeable difference between the two outbreaks was the presence of a deeper mid-level shortwave trough over Ohio Valley during the 2016 event (Figure 1a). The trough during the 2012 event is weaker and, more importantly, stronger anticyclonic circulation exists directly south of the trough/short wave (Figure 1b), which boosts moisture supply transported from the Gulf of Mexico. The location of the short wave (Figure 1b) and MP corridor is shifted north in the 2012 case (Figure 3b) compared to the 2016 case (Figure 3a). The deeper trough at mid-level perhaps led to the staggering precipitation generated in 2016 but not in 2012. There are numerous documented cases where NWF events produced MP-related severe weather outbreaks (e.g. Johns and Hirt 1987; Bentley and More 1988); oftentimes, NWF events fail to produce such outbreaks as was the case during the historical drought of June 1988, when the ridge and NWF pattern were both present, but little MP activity was observed downstream of the ridge (Figure 3c).

4.2 Climatology and variability of MPs

As studies have shown impacts from anthropogenic climate change across North America have become discernable starting around the mid-1980s (King et al. 2015; Christidis et al. 2013), we considered data from 1985 to 2016 to evaluate the MP climatology and interannual variability. As shown in Figure 2, the 32-year MP climatology shows similar pattern with the 10-year, manually tracked MP climatology by Wang et al. (2011a, b). The spatial distribution of the MP climatology developed here is also in good agreement with the mid-summer derecho frequency previously documented (Guastini and Bosart 2016; John and Hirt 1987). We then compared the MP climatology with the SPC storm report (wind and hail) for the same period and found the storm frequency (Figure 4) during the NWF outbreak matches well with the MP frequency (Figure 2). Generally, storm frequency is greater in July (Figure 4b) compared to June frequency (Figure 4a). It was also observed that following the northward shift of the jet stream, both MP frequency and storms correspondingly shift northward from June to July. Consistent with previous studies (Bentley and Mote 1998; Johns and Hirt 1987), the spatial distribution pattern shows that more frequent storms were reported in the northern Plains during the NWF outbreak. However, because of the previously mentioned limitations and biases associated with storm reports, this result should be interpreted cautiously.

Next, we examined the June-July patterns of MP interannual variability. Since the empirical orthogonal function (EOF) analysis provides the spatial modes/patterns of variability and how they change with time (Hannachi 2004; Monahan et al. 2009), the EOF analysis was applied on the MP frequency. The result reveals three leading modes (Figure 5), which constitute more than 50% of the total variance. The first mode explains 23% of the total variance, comparable with the second mode (21%) and considerably larger than the third mode (8%). EOF2 shows the north and south fluctuation of the MP corridor (Figure 5b) while EOF3 depicts the east-west oscillation of MP corridor (Figure 5c). The first and third modes, in particular, are highly comparable to the 2016 events, revealing the MP corridor that resembles the West Virginia case encompassing the Upper Midwest main track (EOF1) and the increased frequency in the East Coast (EOF3). We also note that the north-south shift of MP corridor is reflected in EOF2 and it resembles the 2012 storm track with a high principal component (PC) value (not shown).

For evaluation purposes, we examined the correlation of the PC time series with storm frequency, mid-level height, and surface temperature (Figure 6). Here we consider all three PCs (PC1, PC2 and PC3) to analyze the correlation pattern as these three PCs most resemble the most recent extreme events. The PC1 correlates well with the storm frequency (Figure 6a) along the main MP corridor. The PC2 positively correlates with the storm frequency that occurred in the north while correlation is stronger (but negative) on the south side (Figure 6b). PC3 correlates with the eastward shift of the extreme weather (Figure 6c). The correlation map of 600-hPa geopotential height with PC1 (Figure 6d) shows a predominant anticyclone centered in the southern U.S. providing enhanced NWF conditions over the northern plains, upper Midwest, and Ohio Valley, while low pressure over the Great Lakes diminishes the MP generation process. Furthermore, the PC1 is highly correlated with an increased meridional gradient of mid-level height over the U.S. These features lend support to the criteria utilized to depict the MPs, the associated stormy weather activity, and the underlying circulation pattern.

It is noteworthy that the PC2 correlation with 600-hPa height shows a northward shift of the high-pressure ridge accompanied by the northward shift of severe weather events during the high PC2 (Figure 6e). The example of extreme weather that corresponds to this shift is the 2012 derecho event (Figure 1b). By comparison, PC3 is positively correlated only with an increased meridional gradient of the geopotential height over the mid-Atlantic region (Figure 6f) and this corresponds with the increased storm frequency and warmer air in the southeast U.S. (Figure 6i). Surface air temperature in the southern U.S. increases correspondingly with EOF1 (Figure 6g) and it too coincides with the two warmer-than-normal seasons in the southwest U.S. during June 2012 and 2016. This temperature pattern also implies increased meridional temperature gradient along the NWF zone. The PC2 correlation with surface temperature (Figure 6h) coincides with the shifting of high pressure northward (Figure 6e). We further correlated the PC1 with the Gulf of Mexico sea surface temperature (SST) using ERSSTv4 data for different months and observed that MP activity responds to Gulf SST conditions during the early summer months (not shown).

When Gulf SSTs are anomalously warm, the ridge of high pressure located over the south central U.S. responds by strengthening—leading to a positive correlation between MP activity and Gulf SST conditions. Furthermore warmer Gulf sea surface enhances the atmospheric moisture supply over the MP region.

4.3 Linear trend of MPs, storms and convective precipitation

With severe convective storms recently occurring more frequently as the climate warms (King et al., 2015), it is worthwhile to check the trend of a few variables contributing to the MP environment. The time series of PC1, MP index and Gulf of Mexico sea surface temperature (SST) averaged for June and July are shown in Figure 7. Both PC1 and the MP index show an increasing trend (Figure 7a and b). We note the high confidence level ($p<0.01$) observed for the steadily increasing Gulf of Mexico SST trend (Figure 7c). Figure 7d shows the distribution of weekly averaged MP event over Ohio region for the 32 years and shows that more MP events are occurring in recent years.

To examine the geographical distribution, we next computed the linear trend maps in MPs and storm frequency for June and July along the MP corridor during the period from 1985 to 2016 (Figure 8). A substantial increase to northern plain MP activity is noted (Figure 8a). Storm frequency trends also indicate the increasing activity along the MP corridor (Figure 8b) and we note that the increasing trend is greater in June compared to July (figure not shown). Since PC1 is correlated with the high pressure over the south-central U.S., the trend of the mid-level pressure fields reveals a marked increase over the same region (figure not shown) and this agrees with the climatological study by Vavrus et al. (2017), which showed that increasing temperature trends, and by association, the central U.S. summertime ridge of high pressure promotes more intense summer weather.

By using the NARR output of convective precipitation, we computed its trends to assess the change in convective activity (Figure 8c). Again, increasing trends were found along the MP corridor, although the significance level is marginal. It is possible that MPs are either mostly associated with windstorms or some extreme precipitation events and so, an increase in MPs does not necessarily translate into proportional increase in precipitation. The result should be interpreted cautiously, mainly because most reanalysis products are not homogenized since they have varying observation systems assimilated over time and struggles to accurately portray convective precipitation (Cui et al. 2017).

4.4 Comparison of MP with NARCCAP

Acknowledging the limitations of reanalysis data, the second set of data used in this analysis employed a combination of both reanalysis and climate modeling. Here, the NARCCAP historical run forced by the NCEP data (i.e. reanalysis-driven) was used to calculate the MPs over the same June-July period up to 2003 (see Section 3.2). Three reanalysis-driven NARCCAP models (CRCM, WRFG, and MM5I) were compared with the NARR result. The MPs climatology averaged for June-July is shown in Figure 9a. By comparison, the reanalysis-driven NARCCAP depiction of MPs (Figure 9b) shows a slight northward shift of MPs. MP trend analysis from 1980 to 2003 (Figure 9c and d) produced similar trends between datasets with decreasing trends in MP occurrence along the NWF region, mainly along the Midwest and Mid-Atlantic region, and an increasing trend just east of the Rockies and over the northern Great Lakes.

To further test the effectiveness of the MP metrics across each reanalysis-driven simulations, we evaluated the historical interannual variability. Figure 10 shows the three leading EOF modes of MPs with the NARR and reanalysis-driven NARCCAP ensemble for the month of June and

July. Similar patterns are observed in these EOFs among the two data sets. The EOF1 pattern from both data sources is comparable and represents about 30% of the total variance (upper panel, Figure 11). A similar north-to-south shift of the MP corridor is revealed in EOF2 of both NARR and NARCCAP (middle panel, Figure 11), however this signal is more predominant in NARCCAP where 26% of total variance is explained compared to NARR's 17%. While each EOF3 represents roughly the same variance, slightly different spatial patterns were found (lower panel, Figure 11).

4.5 Climate Projection

With the establishment of the MP tracking algorithm, and the good agreement between reanalysis-driven NARCCAP data and NARR reanalysis, we proceeded to examine the future climate projection of MPs considering the global model-driven NARCCAP data. The climatology of MPs for the June-July average using historical and future runs from the ensemble of three models (six simulations) are shown in Figures 10a and 10b, respectively. The spatial distribution of the MP climatology from global model-driven historical runs is also in good agreement with the reanalysis data (Figure 2). For individual months (see supplementary Figure S1), July features a higher frequency and a northward shift in the MP track compared to June, which is also consistent with the reanalysis result. However, the simulated 600-hPa ridge over the southcentral U.S. is weaker for both June and July compared to the NARR.

The future climate projections reveal marked increases in the MP frequency (Figure 11b) while their differences (future minus historical) outline the most notable increase around the Great Lakes region (Figure 11c). The change in the future convective precipitation is shown in Figure 11d, which also depicts an increase in the similar region. A further diagnosis by plotting the low-level jet (considered positive meridional wind) extension during the two periods of time (contours in Figure 11c and d) suggests that the low-level jet (LLJ) is projected to expand northward reaching the corridor of enhanced MPs. Even though the shift appears small, the close proximity between the northern periphery of the LLJ and the southern extent of the MP corridor means the strength of the coupling between the two phenomena is quite sensitive to even minor displacement. This notion of a strengthened low-level jet echoes the global climate model projection by Cook et al. (2008) and Weaver et al. (2009), as well as the observed historical intensification by Barandiaran et al. (2013). Individual model simulations of these features are shown in the supplemental Figure S1. Combined, the projection that the enhanced MP activity may interact with the strengthened low-level jet helps explain the projected increase – more than doubling – of the summertime convective rainfall across the Ohio River Valley and Mid-Atlantic U.S.

5. Concluding Remarks

Existing global climate models and regional climate models operate at coarser horizontal and vertical resolutions and currently cannot resolve deep convection accurately through convection parameterization schemes (Prein et al. 2015). However, even high-resolution convection-permitting models used in dynamical downscaling also underestimated MCSs that form within the background mid-level NWF (Prein et al. 2017). Climate models also have a difficulty producing weakly-forced storms and any resultant extreme precipitation and this drawback may affect how the models project future climate extremes. To understand the extent to which devastating floods like the one in West Virginia, a NWF type of storm, will occur relies on how well climate models depict the NWF synoptic settings and embedded MPs. The present study of the MP climatology has developed metrics that can identify and evaluate NWF severe weather outbreaks in the large-ensemble, multi-model projections. The developed metrics is tested for two summer months (June and July), utilizing both the reanalysis and regional downscaling datasets to evaluate the model depiction and projections for future extreme weather climatology associated with the NWF environment over the northern part of the U.S.

The following observations were made from this study:

1) Convective outbreaks associated with NWF events are occurring more frequently in recent years, mainly after 1980, suggesting that the global climate change is potentially impacting the MP frequency and intensity and associated extreme weather.
2) The Gulf of Mexico SST and mid-level high pressure over the central U.S. show strong correlation with MPs and both of these regional features have intensified, as well.
3) Regional climate models with a 50-km spatial resolution do capture the NWF synoptic setting and subsequently, the MP location and frequency. The MP climatology from historical climate simulations shows a good agreement with the observation-based reanalysis data.
4) Future climate simulations reveal that both the MP frequency and associated convective precipitation will increase during June and July over the MP corridor.

Future work should focus on examining the extent to which higher-resolution models, preferably at the convection permitting resolution (3 to 4 km), depict and project the weakly-forced/NWF type of summer convective storms for North America. Future work will be extended the analysis period over the full summer months (May-Sep) utilizing other reanalysis data and climate data to find the MP climatology, trend and variability.

Acknowledgement: This research was supported by the US Department of Energy grant DESC0016605 and the Utah State University Agricultural Experiment Station, under paper 9129. Comments provided by two anonymous reviewers were valuable and are highly appreciated.

References

Barandiaran, D., S.-Y, Wang, and K. Hilburn, 2013: Observed trends in the Great Plains low-level jet and associated precipitation changes in relation to recent droughts. Geophysical Research Letters, 40, 6247-6251.

Berg, L.K, L.D. Riihimaki, Y. Quan, H. Yan, and M. Huang, 2015: The low-level jet over the southern Great Plains determined from observations and reanalysis and its impact on moisture transport. J. Climatol., 28, 6682-6706.

Bentley, M.L. and T.L. Mote, 1998: A climatology of derecho-producing mesoscale convective systems in the central and eastern United States, 1986-95. Part I: Temporal and spatial distribution. Bull. Amer. Meteor. Soc., 79, 2527-2540.

Christidis, N., P.A. Stott, G.C., Hegrel, and R. A. Betts, 2013: The role of land use change in recent warming of daily extreme temperatures, Geophysical Research Letters, 40, 589-594.

Cook, K.H., E.K. Vizy, Z.S. Launer, and C.M. Patricola, 2008: Springtime intensification of the Great Plains low-level jet and Midwest precipitation in GCM simulations of the twenty-first century. Journal of Climate, 21, 6321-6340.

Corrigan, P., S. J. Keighton, R. Stonefield, and R. H. Grumm, 2017: The West Virginia Historic and Devastating Floods of 23 June 2016: Summary of Impacts and National Weather Service Decision Support Services. 97th AMS Annual Meeting, Seattle, WA, 22-27 Jan 2017.

Cui, W., X. Dong, B. Xi, and A. Kennedy, 2017: Evaluation of Reanalyzed Precipitation Variability and Trends Using the Gridded Gauge-Based Analysis over the CONUS. Journal of Hydrometeorology, 18(8), 2227-2248.

Di. Liberto, T., 2016: Scorching heat breaks the Southwest in mid-June 2016. Retrieved from https://www.climate.gov/news-features/event-tracker/scorching-heat-bakes-southwest-mid-june-2016.

Feng., Z., L.R. Leung, S. Hagos, R.A. Houze, C.D. Burleyson, and K. Balaguru, 2016: More frequent intense and long-lived storms dominate the springtime trend in central US rainfall, Nature Communications, 7:13429, DOI: 10.1038/ncomms13429.

Feng, Z., X. Dong, B. Xi, S.A. McFarlane, A. Kennedy, B. Lin, and P. Mannis, 2012: Life cycle of midlatitude deep convective systems in a Lagrangian framework, J. Geophys. Res., 117, D23201, doi:10.1029/2012JD018362.

Galarneau Jr, T.J. and L.F. Bosart, 2005, August. Ridge rollers: Mesoscale disturbances on the periphery of cutoff anticyclones. In Preprints, 21st Conf. on Weather Analysis and Forecasting/17th Conf. on Numerical Weather Prediction, Washington, DC, Amer. Meteor. Soc.

Gallus W.A., N.A. Snook, and E.V. Johnson, 2008: Spring and summer severe weather reports over the Midwest as a function of convective mode: a preliminary study. Weather Forecast, 23:101–113

Grote, T. and J.L. Dyer, 2017: Preliminary Assessment of the Hydrometeorology and Hydrology of the June 2016 Greenbrier River Flooding, West Virginia. 97th AMS Annual Meeting, Seattle, WA, 22-27 Jan 2017.

Grumm, R., 2017: A Model Review of the Historic West Virginia Historic and Devastating Floods of 23 June 2016. 97th AMS Annual Meeting, Seattle, WA, 22-27 Jan 2017.

Guastini, C.T. and L.F. Bosart, 2016: Analysis of a progressive derecho climatology and associated formation environments. Mon. Weather Rev., 144, 1363-1382.

Hannachi A., 2004: A Primer for EOF Analysis of Climate Data. Department of Meteorology, University of Reading: Reading, UK, 33 pp.

Jiang, X., N.-C. Lau, and S.A. Klein, 2006: Role of eastward propagating convection systems in the diurnal cycle and seasonal mean of summertime rainfall over the U.S. Great Plains. Geophys. Res. Lett., 33, L19809, doi:10.1029/2006GL027022.

Johns R.H., 1982: A synoptic climatology of northwest flow severe weather outbreaks. Part I: nature and significance. Mon. Weather Rev., 110, 1653–1663.

Johns R.H., 1984: A synoptic climatology of northwest flow severe weather outbreaks. Part II: meteorological parameters and synoptic patterns. Mon Weather Rev 112:449-464.

Johns R.H., 1993: Meteorological conditions associated with bow echo development in convective storms. Weather Forecast, 8, 294–299.

Johns R.H., Hirt W.D., 1987: Derechos: widespread convectively induced windstorms. Weather Forecast, 2, 32–49.

Kalnay, E., and Coauthors, 1996: The NCEP/NCAR 40-Year Reanalysis Project. Bull. Amer. Meteor. Soc., 77, 437-471.

King, A.D., M.G. Donat, E.M. Fisher, E.H. Hawkins, L.V. Alexander, D.J. Karoly, A.J. Dittus, S.C. Lewis, and S.E. Perkins, 2015: The timing of anthropogenic emergence in simulated climate extremes. Environ. Res. Lett., 10, 094015, doi:10.1088/1748-9326/10/9/094015.

Mearns, L. O., et al. (2009), A regional climate change assessment program for North America, *Eos Trans. AGU*, **90**(36), 311.

Mesinger F. et al., 2006: North American regional reanalysis. Bull. Am. Meteorol. Soc., 87, 343–360.

Mo, K. C., and D. P. Lettenmaier, 2015: Heat wave flash droughts in decline. Geophysical Research Letters, 42(8), 2823-2829.

Monahan, A., J. C. Fyfe, M. H. Ambaum, D. B. Stephenson, and G. R. North, 2009: Empirical orthogonal functions: The medium is the message, *J. Clim.*, **22**, 6501–6514.

NOAA, National Centers for Environmental Information, State of the Climate: Synoptic Discussion for June 2016, published online July 2016, retrieved on July 19, 2017 from https://www.ncdc.noaa.gov/sotc/synoptic/201606.

Perfater, S., B. Albright, J. Kastman, M. Klein, and M.J., Erikson, 2017: Testing the utility of high-resolution convection-allowing models at longer time scales to improve excessive rainfall outlooks at NOAA's weather prediction center. 97th AMS Annual Meeting, Seattle, WA, 22-27 Jan 2017.

Prein, A.F., C. Liu, K. Ikeda, R. Bullock, R.M. Rasmussen, G.J. Holand, and M. Clark, 2017: Simulating North American mesoscale convective systems with a convection-permitting climate model. Climate Dynamics, DOI 10.1007/s00382-017-3993-2.

Prein et al., 2015: A review on regional convection-permitting climate modeling: Demonstrations, prospects, and challenges. Review of Geophysics, 53, 323-361.

Schwartz, C.S., G.S. Romine, R.A. Sobash, K.R. Fossell, and M.L. Weisman, 2016: NCAR's experimental real-time convection-allowing ensemble prediction system. Weather and Forecasting, 30(6), 1645-1654.

Šepić, J., and A. B. Rabinovich, 2014: Meteotsunami in the Great Lakes and on the Atlantic coast of the United States generated by the “derecho” of June 29–30, 2012, Natural hazards, 74(1), 75-107.

Tetzlaff G., Zimmer J., 2013: Probable Maximum Precipitation (PMP). In: Bobrowsky P.T. (eds) Encyclopedia of Natural Hazards. Encyclopedia of Earth Sciences Series. Springer, Dordrecht

Vavrus, S.J., F. Wang, J.E. Martin, J.A. Francis, Y. Peings, and J. Cattiaux, 2017: Changes in North American atmospheric circulation and extreme weather: Influence of Arctic amplification and northern hemisphere snow cover. J. Climate, 30, 4317-4333.

Wang, S.-Y., R. R. Gillies, E. S. Takle, and W. J. Gutowski Jr., 2009: Evaluation of precipitation in the Intermountain Region simulated by the NARCCAP regional climate models. *Geophys. Res. Lett.*, 36, L11704.

Wang S.-Y., Chen T.C. and Taylor S.E., 2009: Evaluations of NAM forecasts on MP-induced convective storms over the U.S. Northern Plains. Weather Forecast, 24, 1309–1333. doi:10.1175/2009WAF2222185.1

Wang, S.-Y., T.-C. Chen, and J. Correia, 2011a: Climatology of summer midtropospheric perturbations in the U.S. northern plains. Part I: influence on northwest flow severe weather outbreaks. Climate Dynamics, 36, 793-810.

Wang, S.-Y., T.-C. Chen, and E.S. Takle, 2011b: Climatology of summer midtropospheric perturbations in the U.S. northern plains. Part II: large-scale effects of he Rocky Mountains on genesis. Climate Dynamics, 36, 1221-1237.

Weaver, S.J., S. Schubert, and H. Wang, 2009: Warm season variations in the low-level circulation and precipitation over the central United States in observarions, AMIP simulations, and idealized SST experiments. Journal of Climate, 22, 5401-5420.

Weaver, S.J., S. Baxter, and K. Harnos, 2016: Regional changes in the interannual variability of U.S. warm season precipitation. J. Clim., 29, 5157-5173.

Weiss S.J., J.A. Hart, and P.R. Janish, 2002: An examination of severe thunderstorm wind report climatology: 1970–1999. 21st conference on severe local storms, San Antonio, TX, 14 August 2002.

Table 1: Regional climate models and forcing data used in this study. Two historical runs are considered; one is driven by global model and other by reanalysis data.

Regional climate model	Forcing data		Historical run		Future run
	global model	reanalysis	global model-driven	reanalysis-driven	
CRCM	CCSM3 and CGCM3	NCEP	1968-1999	1980-2003	2038-2069
MM5I	CCSM3* and HadCM3	NCEP	1968-1999	1980-2003	2038-2069
WRFG	CCSM3 and CGCM3	NCEP	1968-1999	1980-2003	2038-2069

*the MM5I-CCSM3 has the data from 1968-1998 only for historical run.

Table 2: List of acronyms used in the manuscript

Abbreviation	Full name
MP	Mid-tropospheric perturbation
MCS	Mesoscale Convective System
NARR	North American Regionals Reanalysis
NARCCAP	North American Climate Change Assessment Program
WCM	Warning Coordination Meteorologist
SPC	Storm Prediction Center
NWF	North Westerly Flow
EOF	Empirical Orthogonal Function
PC	Principal Component
SST	Sea Surface Temperature
ENSO	El Niño–Southern Oscillation

PDO	Pacific Decadal Oscillation
NAO	North Atlantic Oscillation
AO	Arctic Oscillation
PNA	Pacific North America
AMO	Atlantic Multidecadal Oscillation

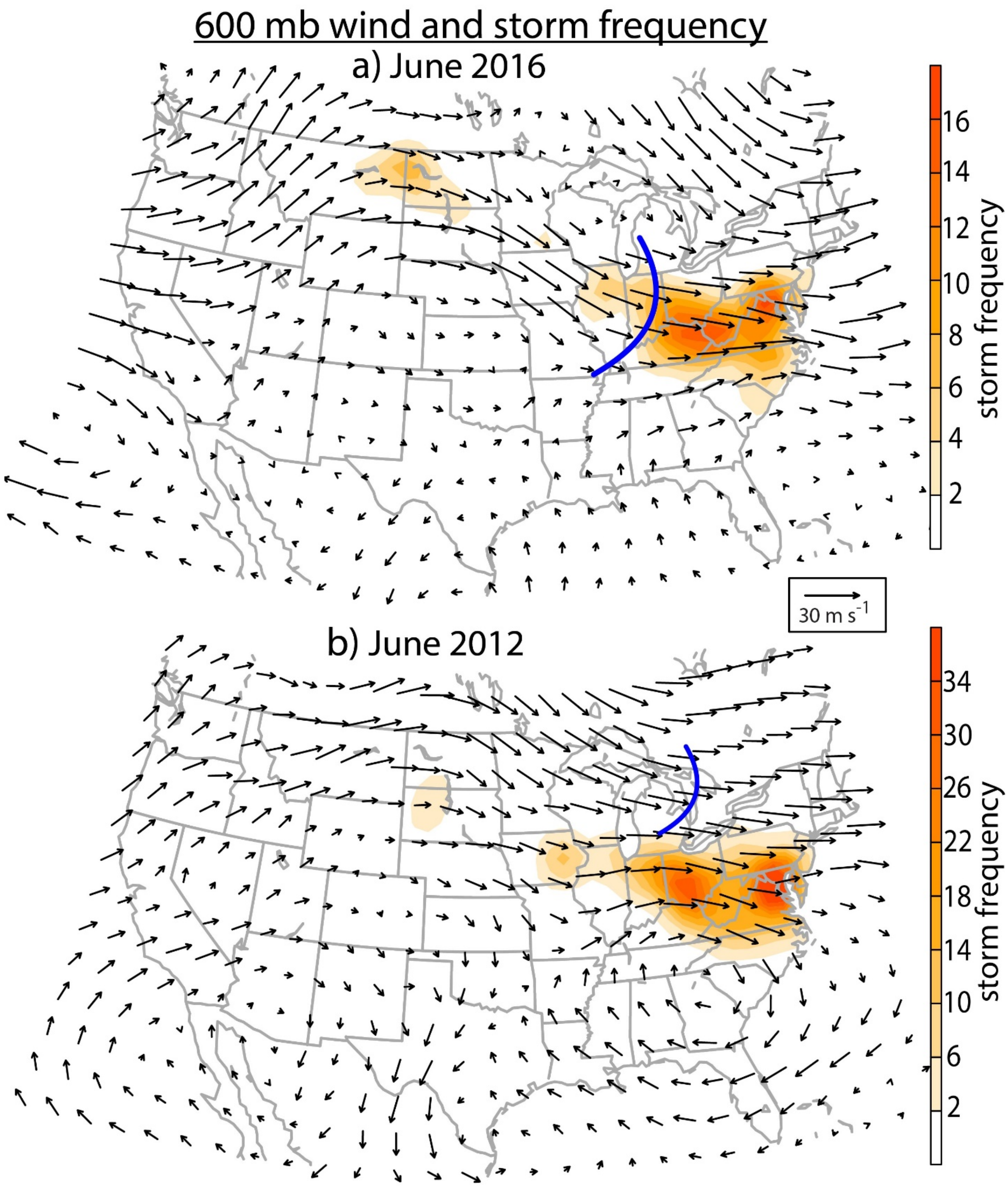

Fig. 1 Wind vectors at 600 mb and storm (wind and hail) frequency (shaded) from storm reports. a) Wind vectors from 18Z on 23 June 2016 and total storm reports for 21-24 June 2016. b) Wind vectors from 03Z on 30 June 2012 and total storm reports for 28-30 June 2012. Blue curve in both panels shows the location of the shortwave trough.

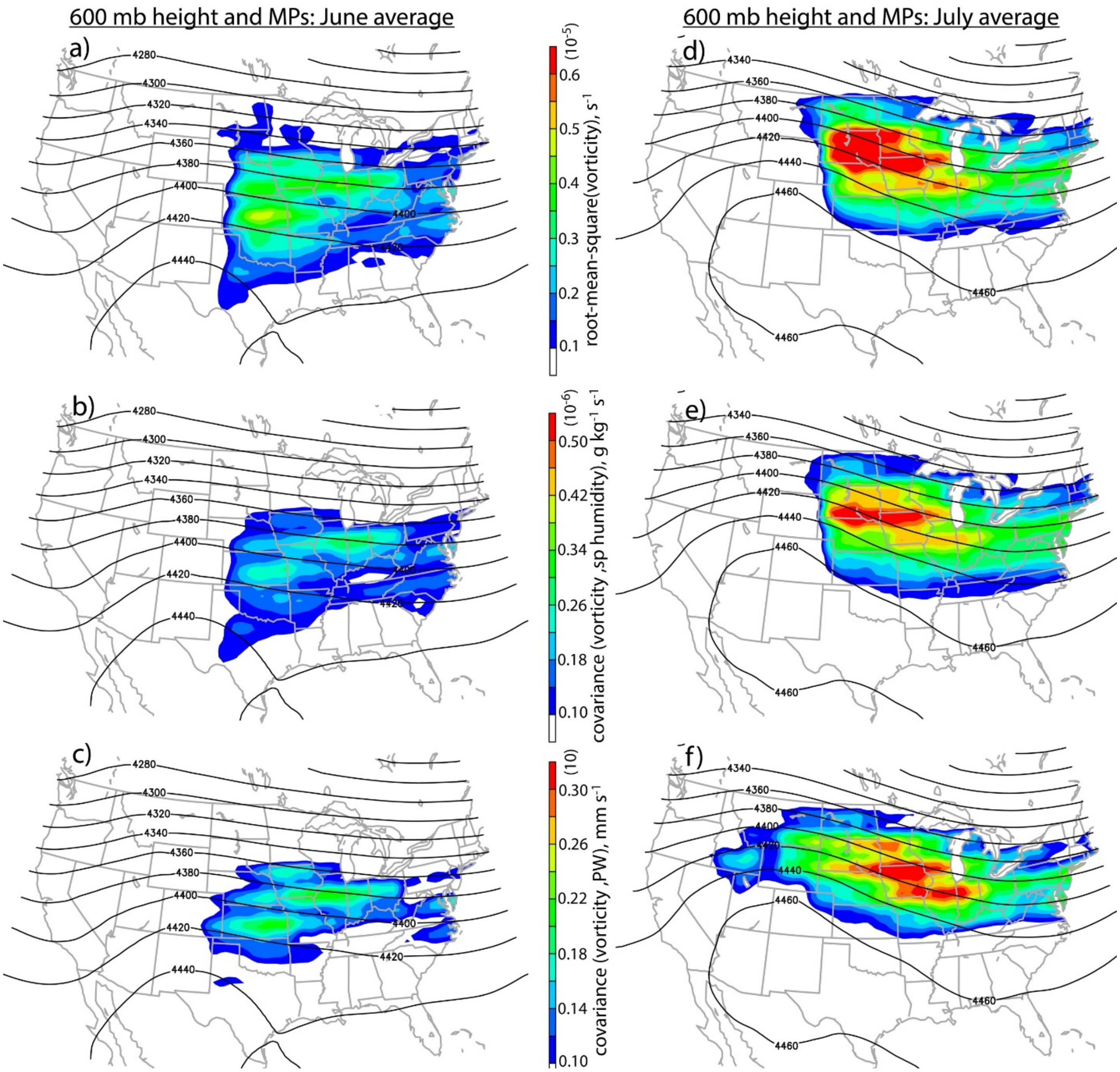

Fig. 2 Climatology (1985-2016) of MPs based on three different methods (defined in text) for June (left panels) and for July (right panels). Color shaded in a) and d) are the root-mean-square of 600-hPa vorticity, b) and e) are the covariance of 600-hPa vorticity and 300-hPa specific humidity, and c) and f) are the covariance of 600-hPa vorticity and vertically integrated precipitable water. Contours in all panel are the average 600-hPa height.

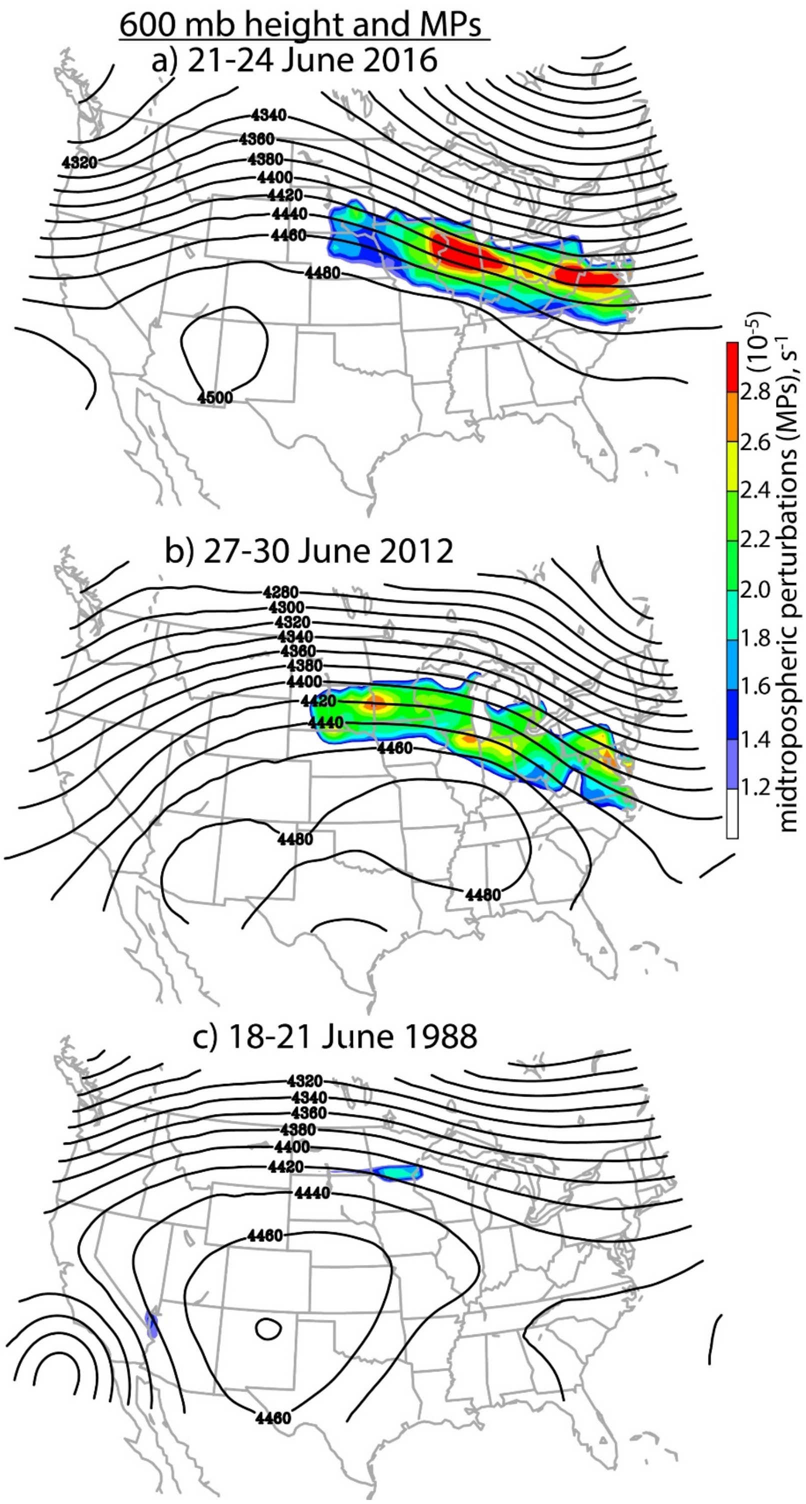

Fig. 3 Height contours at 600 mb and MPs (shaded) averaged for a) 21-24 June 2016, b) 27-30 June 2012, and c) 18-21 June 1988.

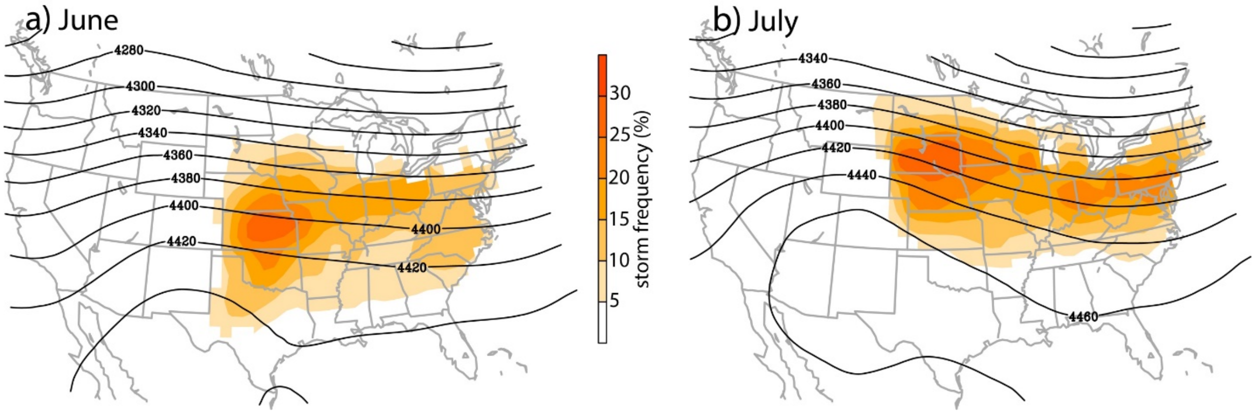

Fig. 4 Climatology (1985-2016) of storm frequency with 600-hPa height contours. Left panel shows the average for June and right panel shows the average for July.

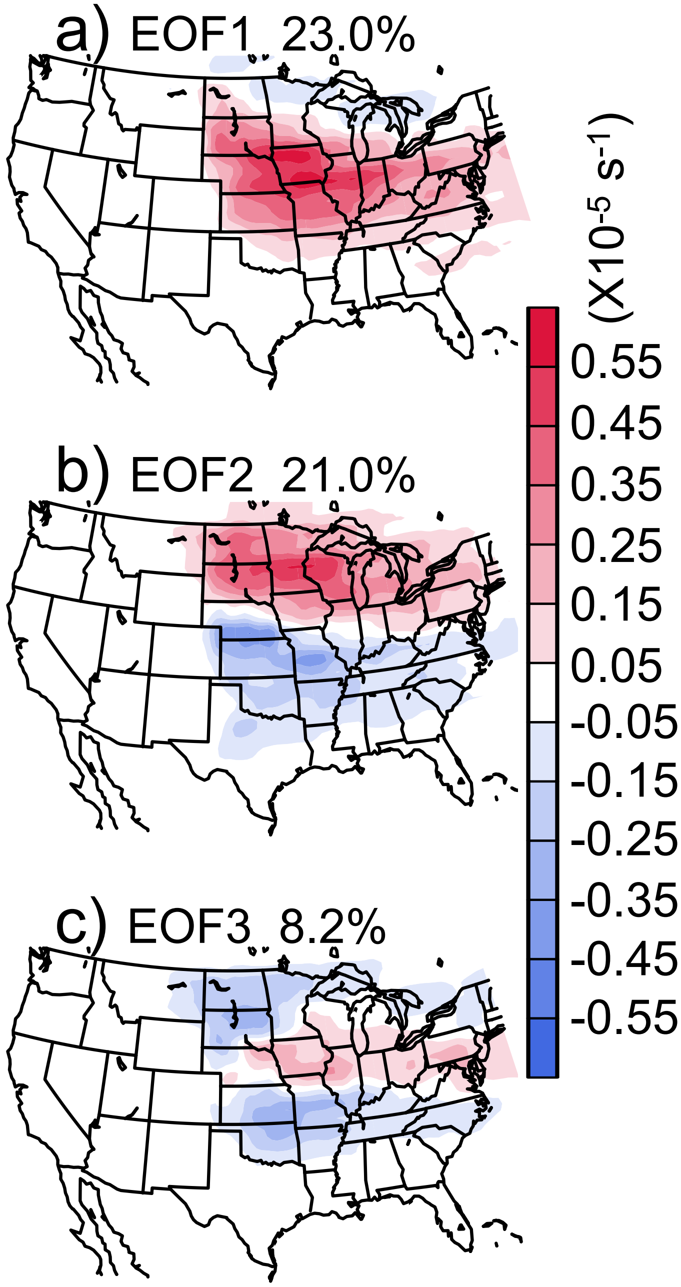

Fig. 5 Three modes of Empirical Orthogonal Functions (EOFs) of MPs averaged for June and July from 1985 to 2016. a) EOF1, b) EOF2, and c) EOF3 with percentage of variance.

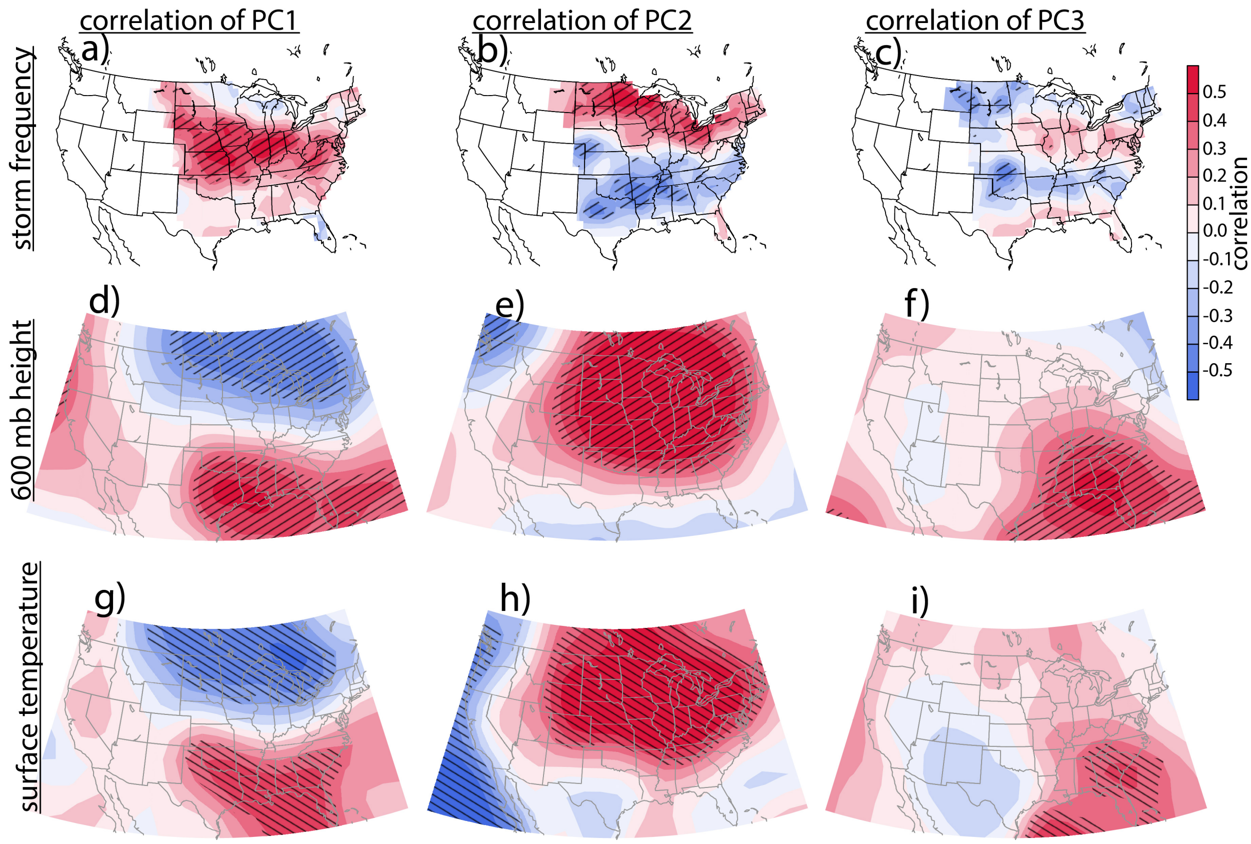

Fig. 6 Temporal correlation of PC1 (left panel), PC2 (middle panel) and PC3 (right panel) with storm frequency (a, b and c), 600-hPa geopotential height (d, e and f), and surface (2m) temperature (f, h, and i), respectively. Hatched areas indicate significant values with $p<0.05$.

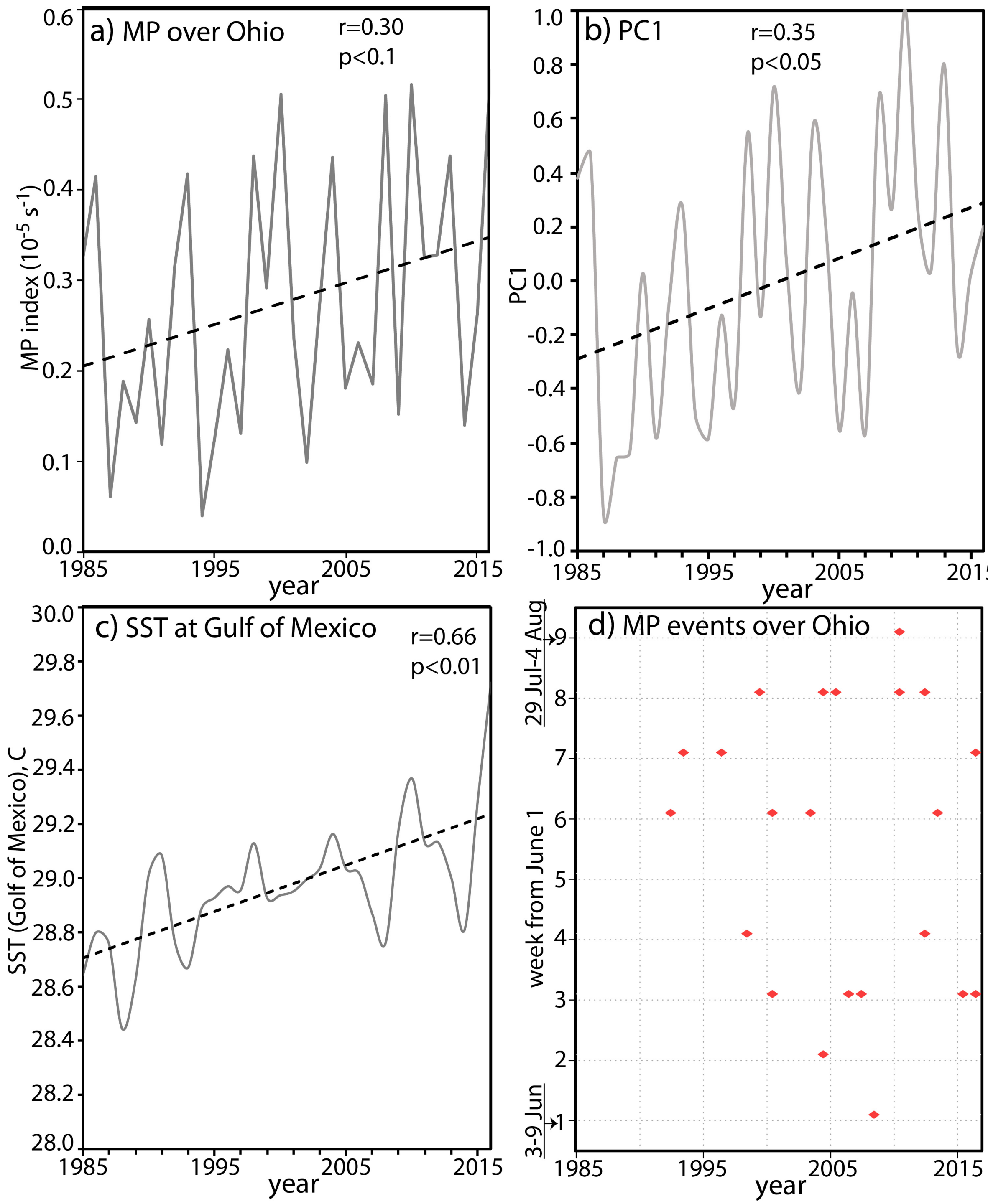

Fig. 7 Gray line shows the timeseries of a) MP over Ohio (within 6X6 deg box centered over Ohio), b) PC1, and c) sea surface temperature (SST) from NOAA extended reconstructed V4 at Gulf of Mexico from 1985 to 2016. All three variables in a), b) and c) are averaged for June and July and the dashed line is the trend line and correlation coefficient (r) and p-value are given for each plot. Lower right panel d) shows the distribution of MP events over the Ohio region for same period. The MP activity is considered when the weekly average MP over Ohio region is larger than 10^{-5} s^{-1}.

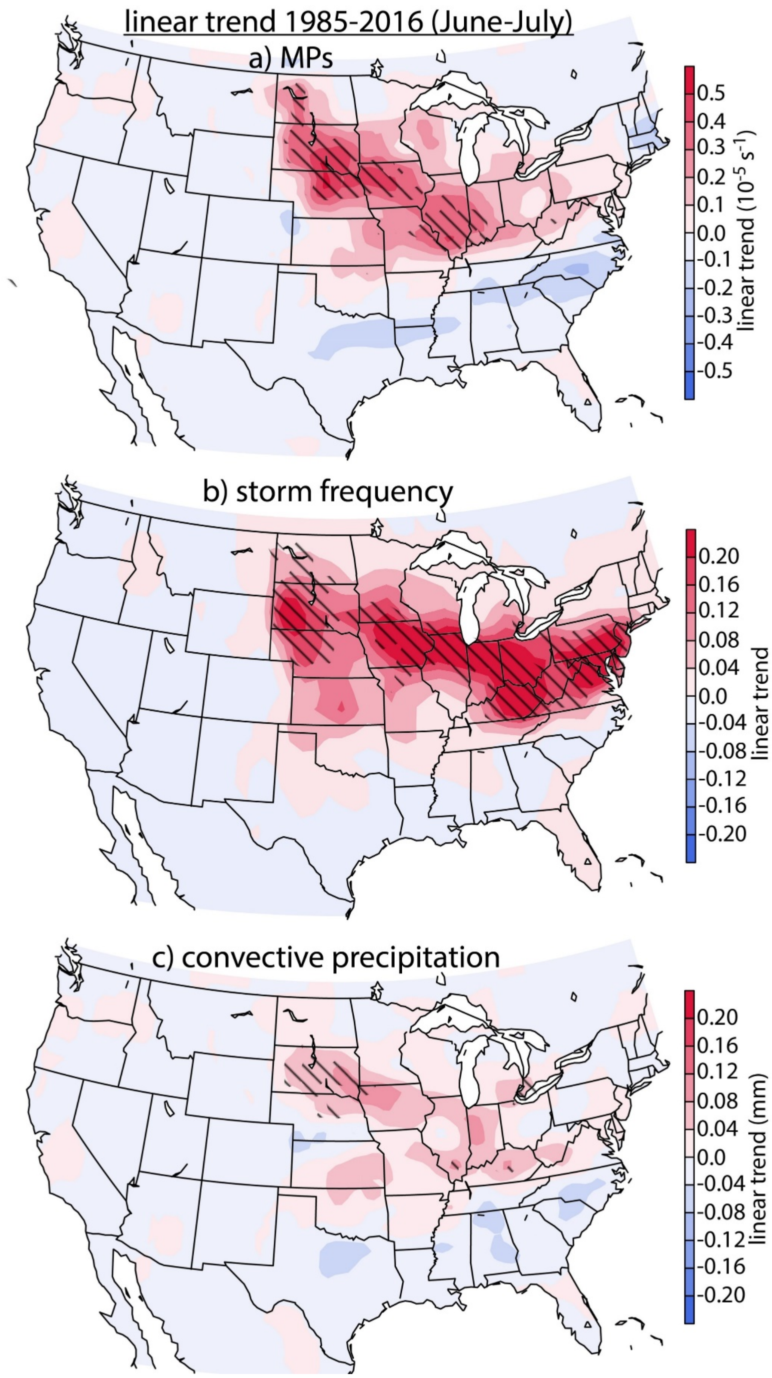

Fig. 8 Linear trend (slope times number of years) of a) MPs, b) storm frequency, and c) convective precipitation averaged for June and July from 1985 to 2016. Hatched areas indicate significant values with $p<0.05$.

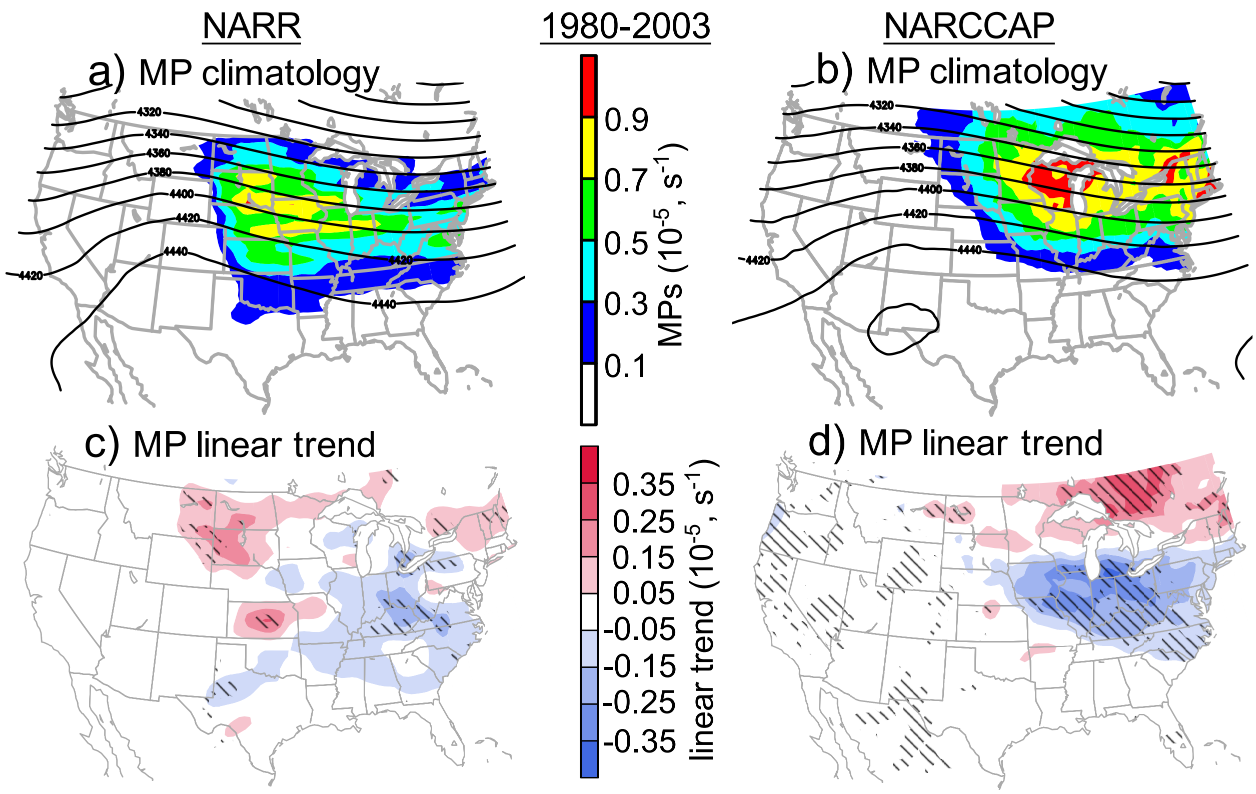

Fig. 9: Average MPs (color filled) and 600-hPa geopotential height (contours) for two months (June and July) a) from NARR data and b) from three historical simulations of NARCCAP data (CRCM, WRFG, and MM5I) forced by NCEP (reanalysis-driven) considering 24 years (1980-2003). Linear trend of average MPs for June and July for the same 24 years period c) from NARR data, and d) from three simulations of reanalysis-driven NARCCAP data. Hatched lines in c) and d) are the significant values with $p<0.1$.

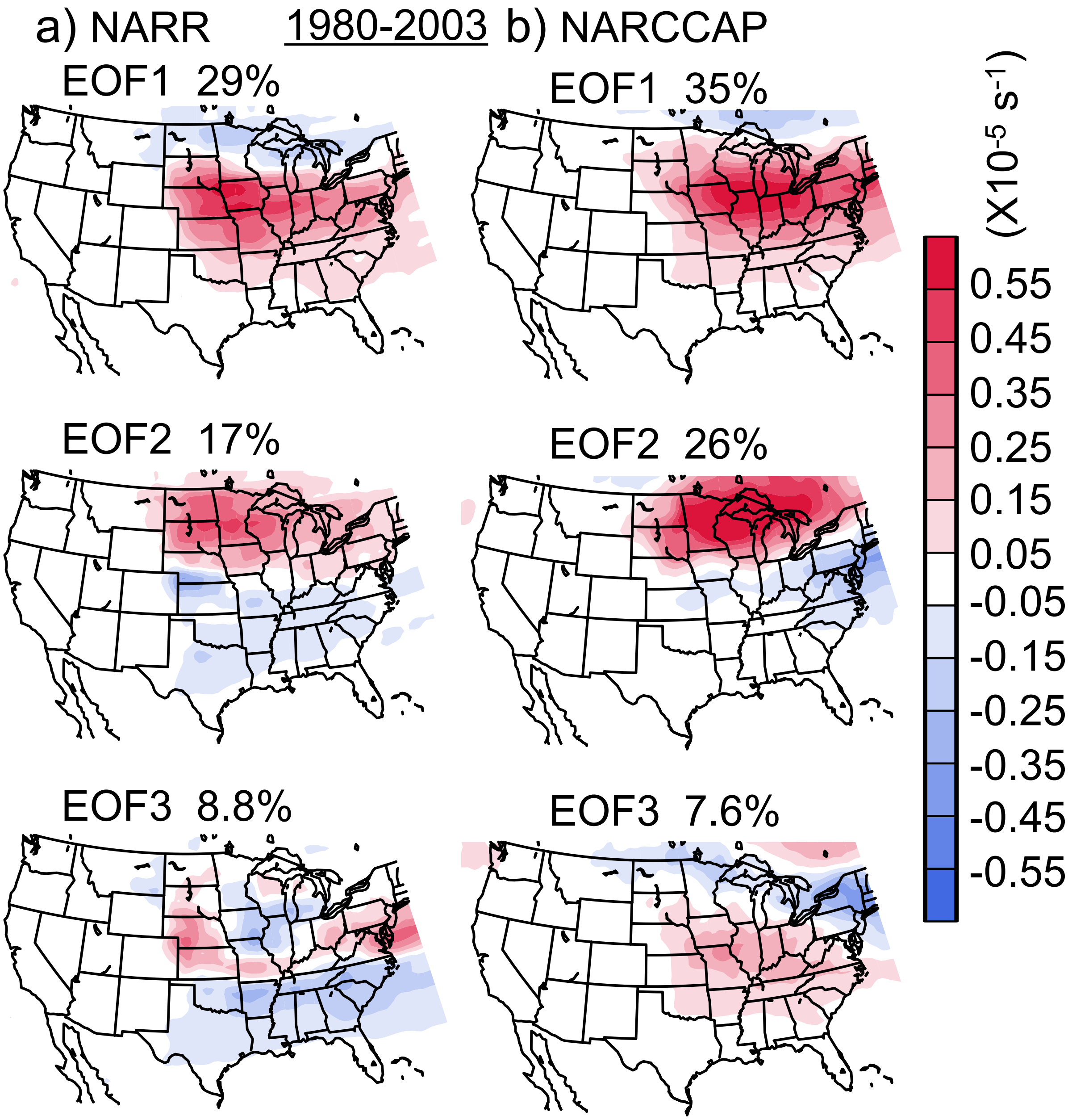

Fig. 10: Three modes of Empirical Orthogonal Functions (EOFs) of MPs averaged for June and July from 1980 to 2003 with percentage of variance from a) from NARR data, and b) from three historical simulations of NARCCAP data (CRCM, WRFG, and MM5I) forced by NCEP (reanalysis-driven).

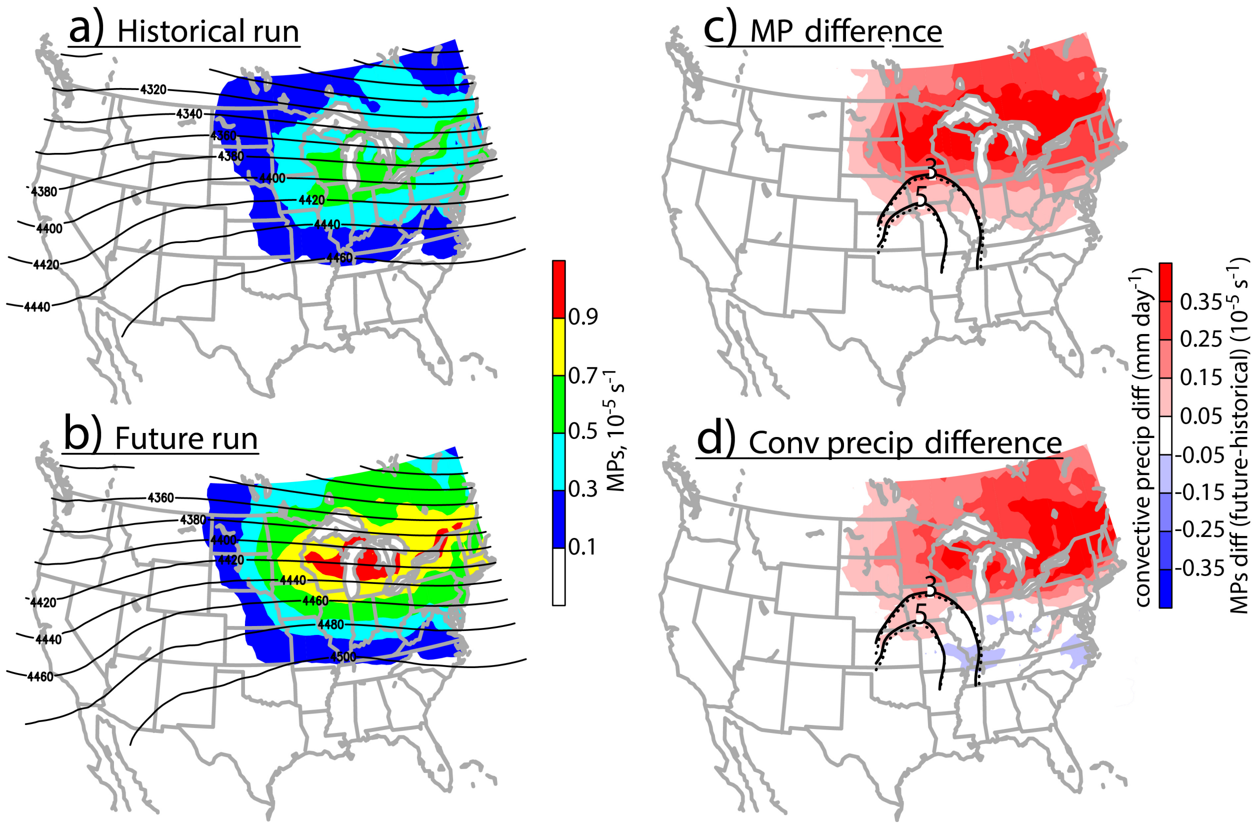

Fig. 11 Average MPs (color filled) and 600-hPa geopotential height (contours) from six model ensembles of NARCCAP data for two months (June and July). a) Historical run from 1969 to 1999, b) future run from 2038 to 2066, and c) difference between future and historical runs of MPs. d) shows the convective precipitation difference between future and historical runs and contours are the positive V-wind at 925 hPa to depict the low-level jet from the historical run (dotted lines) and future run (solid lines) in c) and d). The convective precipitation is considered only from the MP cases. The six simulations used here are CRCM3-CCSM3, CRCM3-CGCM3, MM5I-CCSM3, MM5I-HadCM3, WRFG-CCSM3, and WRFG-CGCM3 from the NARCCAP regional climate modeling.